ROBUST WIDELY LINEAR BEAMFORMING VIA THE TECHNIQUE OF SHRINKAGE FOR STEERING VECTOR ESTIMATION

Jiangbo Liu, Wei Xie, Changsheng Wang, Qun Wan*

School of Electronic Engineering, University of Electronic Science and Technology of China, Chengdu 611731, China. *Corresponding author: wanqun@uestc.edu.cn

ABSTRACT

In this paper, two novel robust widely linear beamforming algorithms based on the technique of shrinkage are proposed, i.e., the WL-RBLW and the WL-OAS. Firstly, in order to remove the signal-of-interest's (SOI's) component from the sample covariance matrix (SCM), the augmented interference-plus-noise covariance matrix (A-IPNCM) is reconstructed based on the spatial spectrum of noncircular coefficient. Then, a modified Rao-Blackwell Ledoit-Wolf (RBLW) estimator and a modified Oracle Approximating Shrinkage (OAS) estimator are developed to directly estimate the desired signal's extended steering vector. Only the prior knowledge of the antenna array geometry and the angular sector in which the desired signal is located are utilized in the proposed algorithms. Compared with several representative robust WL beamformers, numerical simulations demonstrate that the proposed beamformers can achieve a better performance.

Index Terms— Widely linear beamforming, noncircular signal, augmented covariance matrix reconstruction, shrinkage method, signal steering vector estimation

1. INTRODUCTION

Adaptive traditional beamforming techniques have mainly considered the second-order (SO) circular signals [1–4]. Nevertheless, the SO noncircular and nonstationary signals are often encountered in the areas of radio communication and satellite communication, such as amplitude-shift keying (ASK), binary phase-shift keying (BPSK), and unbalanced quaternary phase-shift keying (UQPSK) [4, 5]. For this class of signals, conventional beamforming algorithms, such as minimum variance distortionless response (MVDR) beamformer, are shown to be suboptimal, and the optimal complex filters become widely linear (WL) [6]. In order to exploit the noncircularity of the desired signal, the optimal WL-MVDR beamformer was developed and analyzed in [7] and [2, 8], respectively. However, the optimal WL-MVDR is limited in practical applications since the desired signal's noncircularity coefficient and steering vector (SV) should be known precisely [6]. Therefore, many robust WL beamforming algorithms have been proposed to settle this problem [6, 9–12]. Wang's method [9] can handle the uncertainties of the noncircularity coefficient and array SV, while it is sensitive to the large mismatch of noncircularity coefficient. In addition, two WL-minimum dispersion based beamforming algorithms are proposed by Huang et al. to fully exploit the noncircularity and sub-Gaussian properties of signals [10]. In [11], the noncircular robust Capon beamformer (NC-RCB) is proposed to study the SO noncircularity of both the signal-of-interest (SOI) and interferences. In [12], a robust WL beamformer is proposed on the basis of a projection constraint. As we know, the WL beamformers [9–12] will suffer severe performance degradation at high signal-to-noise ratio (SNR) since the SOI's component is contained in the sample covariance matrix (SCM). In order to further improve the robustness of the WL beamformer at high SNR, the spatial spectrum of noncircularity coefficient is firstly introduced to construct the augmented interference-plus-noise covariance matrix (A-IPNCM) [6]. Moreover, the WL beamformers [6, 10, 12] are difficult to be applied in practical engineering due to their high computational burden.

To avoid high computational cost, two low-complexity robust WL beamformers, i.e., the WL-RBLW and the WL-OAS, are proposed in this paper. Firstly, we propose a new method to calculate the spatial spectrum of the noncircular coefficient, and subsequently reconstruct the A-IPNCM. Then, based on the cross correlation between the observation vector and the WL beamformer's output, a modified Rao-Blackwell Ledoit-Wolf (RBLW) estimator and a modified Oracle Approximating Shrinkage (OAS) estimator are developed to estimate the desired signal's extended steering vector (ESV).

Notation: Matrices (vectors) are denoted by boldface uppercase (lowercase) letters. The superscriptions $*$, T and H denote the conjugate, transpose and Hermitian transpose, respectively. The notations $\mathbf{I}$, $\mathbf{1}$, $E\{\cdot\}$, $\|\cdot\|$, Tr$(\cdot)$, $\langle\cdot\rangle$, $\|\cdot\|_F$ stand for the unit matrix, all-one column vector, expectation, Euclidean norm, trace, the time-averaging operation and the Frobenius norm of a matrix, respectively. diag$(\mathbf{x})$ represents the diagonal matrix with $\mathbf{x}$ in its main diagonal, and diag$(\mathbf{X})$ denotes the column vector whose elements are the diagonal elements of $\mathbf{X}$. $\Theta^a \setminus \Theta^b$ denotes the difference set with the elements of $\left\{x \mid x \in \Theta^a \text{ and } x \notin \Theta^b\right\}$.

2. THE SIGNAL MODEL

Considering an array of N sensors to receive P narrowband signals, the received data can be modeled as

$$\mathbf{x}(t) = \mathbf{a}_1 s_1(t) + \mathbf{v}(t), \tag{1}$$

where $\mathbf{v}(t) = \sum_{p=2}^{P} \mathbf{a}_p s_p(t) + \mathbf{n}(t)$ represents the whole interference-plus-noise (IPN) vector, t denotes the time in-

This work was supported in part by the National Natural Science Foundation of China (NSFC) under Grant U1533125 and 61771108, National Science and technology major project under Grant 2016ZX03001022, and the Fundamental Research Funds for the Central Universities under Grant ZYGX2015Z011.

dex, $\mathbf{n}(t)$ is the noise vector, $s_p(t)$ $(p = 1, 2, \cdots, P)$ is the complex waveform of the p-th signal source. $\mathbf{a}_1$ and $\mathbf{a}_p$ $(p = 2, 3, \cdots, P)$ stand for the true SVs of the SOI and the p-th interference, respectively. The SO statistics of $\mathbf{x}(t)$ are defined by

$$\begin{aligned}\mathbf{R}_x &= \langle E[\mathbf{x}(t)\mathbf{x}(t)^H]\rangle = \sigma_s^2\mathbf{a}_1\mathbf{a}_1^H + \mathbf{Q}_r,\\ \mathbf{C}_x &= \langle E[\mathbf{x}(t)\mathbf{x}(t)^T]\rangle = \gamma_s\sigma_s^2\mathbf{a}_1\mathbf{a}_1^T + \mathbf{Q}_c,\end{aligned} \tag{2}$$

where $\mathbf{Q}_r = \langle E[\mathbf{v}(t)\mathbf{v}(t)^H]\rangle$ and $\mathbf{Q}_c = \langle E[\mathbf{v}(t)\mathbf{v}(t)^T]\rangle$ are the IPN covariance matrix (IPNCM) and the conjugate IPN covariance matrix (C-IPNCM) of $\mathbf{x}(t)$, respectively. $\sigma_s^2 = \langle E[|s_1(t)|^2]\rangle$ and $\gamma_s = \langle E[s_1(t)^2]\rangle/\sigma_s^2 = |\gamma_s|e^{j\phi_s}$ are the power and noncircularity coefficient of the SOI, respectively. When the SOI is the SO noncircular signal ($|\gamma_s| \neq 0$), $s_1^*(t)$ can be decomposed as $s_1^*(t) = \gamma_s^* s_1(t) + [\sigma_s^2(1 - |\gamma_s|^2)]^{1/2}s_1'(t)$ [4], where $s_1'(t)$ is an orthogonal component of $s_1(t)$ with $\langle E[s_1(t)s_1'(t)^*]\rangle = 0$ and $\langle E[|s_1'(t)|^2]\rangle = 1$. Then, the extended vector of $\mathbf{x}(t)$ can be expressed as

$$\tilde{\mathbf{x}}(t) = [\mathbf{x}(t)^T, \mathbf{x}(t)^H]^T = s_1(t)\mathbf{a}_\gamma + \mathbf{v}_\gamma(t), \tag{3}$$

where $\mathbf{a}_\gamma = [\mathbf{a}_1^T, \gamma_s^*\mathbf{a}_1^H]^T$ is the equivalent ESV of the SOI, $\mathbf{v}_\gamma(t) = [\mathbf{v}(t)^T, \mathbf{v}(t)^H + \mathbf{h}(t)^T]^T$ is the global noise vector of $\tilde{\mathbf{x}}(t)$, and $\mathbf{h}(t) = s_1'(t)[\sigma_s^2(1 - |\gamma_s|^2)]^{1/2}\mathbf{a}_1^*$. According to [7], the optimal WL MVDR beamformer is given by

$$\mathbf{w}_{\text{opt}} = [\mathbf{a}_\gamma^H\mathbf{R}_{\mathbf{v}_\gamma}^{-1}\mathbf{a}_\gamma]^{-1}\mathbf{R}_{\mathbf{v}_\gamma}^{-1}\mathbf{a}_\gamma. \tag{4}$$

where $\mathbf{R}_{\mathbf{v}_\gamma} = \langle E[\mathbf{v}_\gamma(t)\mathbf{v}_\gamma(t)^H]\rangle$ denotes the A-IPNCM of $\mathbf{x}(t)$.

3. THE PROPOSED ALGORITHM

3.1. The A-IPNCM Reconstruction

Let Θ stand for the SOI's angular sector, which is assumed to be distinguishable from the locations of the interferences [6, 12–14]. Then, the whole spatial domain Θ_{all} can be divided into two parts, i.e., Θ and its complement sector $\bar{\Theta}$ with $\Theta \cap \bar{\Theta} = \emptyset$ and $\Theta \cup \bar{\Theta} = \Theta_{all}$. Based on the Capon spatial spectrum, the IPNCM can be reconstructed as [13, 15]

$$\tilde{\mathbf{Q}}_r = \int_{\bar{\Theta}} \frac{\mathbf{d}(\theta)\mathbf{d}^H(\theta)}{\mathbf{d}^H(\theta)\hat{\mathbf{R}}_x^{-1}\mathbf{d}(\theta)}d\theta \approx \sum\nolimits_{k=1}^{K} \frac{\mathbf{d}(\theta_k)\mathbf{d}^H(\theta_k)}{\mathbf{d}^H(\theta_k)\hat{\mathbf{R}}_x^{-1}\mathbf{d}(\theta_k)}, \tag{5}$$

where $\hat{\mathbf{R}}_x = (1/L)\sum_{t=1}^{L}\mathbf{x}(t)\mathbf{x}^H(t)$ is the SCM of $\mathbf{x}(t)$, L denotes the number of snapshots, $\theta_1, \theta_2, \cdots, \theta_K$ are the sampled angles in $\bar{\Theta}$, and $\mathbf{d}(\theta_k)$ represents the array SV corresponding to θ_k.

In this paper, the spatial spectrum of noncircular coefficient at direction θ_k is calculated as

$$\gamma(\theta_k) = -\frac{\mathbf{d}^H(\theta_k)\mathbf{E}\mathbf{d}^*(\theta_k)}{\mathbf{d}^H(\theta_k)\mathbf{D}\mathbf{d}(\theta_k)}, \theta_k \in \bar{\Theta},\ k = 1, \cdots, K \tag{6}$$

where $\mathbf{D} = (\hat{\mathbf{R}}_x - \hat{\mathbf{C}}_x\hat{\mathbf{R}}_x^{*\,-1}\hat{\mathbf{C}}_x^*)^{-1}$, $\mathbf{E} = -\mathbf{D}\hat{\mathbf{C}}_x\hat{\mathbf{R}}_x^{*\,-1}$, and $\hat{\mathbf{C}}_x = (1/L)\sum_{t=1}^{L}\mathbf{x}(t)\mathbf{x}^T(t)$ is the conjugate SCM of $\mathbf{x}(t)$. The derivation of $\gamma(\theta_k)$ is obtained by maximizing the WL beamformer's output spatial power $P(\theta_k) = 1/[\mathbf{a}_\gamma^H(\theta_k)\hat{\mathbf{R}}_{\tilde{x}}^{-1}\mathbf{a}_\gamma(\theta_k)]$, where $\hat{\mathbf{R}}_{\tilde{x}} = (1/L)\sum_{t=1}^{L}\tilde{\mathbf{x}}(t)\tilde{\mathbf{x}}^H(t) = \begin{bmatrix}\hat{\mathbf{R}}_x & \hat{\mathbf{C}}_x\\ \hat{\mathbf{C}}_x^* & \hat{\mathbf{R}}_x^*\end{bmatrix}$ is the augmented SCM of $\mathbf{x}(t)$, $\hat{\mathbf{R}}_{\tilde{x}}^{-1} = \begin{bmatrix}\mathbf{D} & \mathbf{E}\\ \mathbf{E}^* & \mathbf{D}^*\end{bmatrix}$, and $\mathbf{a}_\gamma(\theta_k) = [\mathbf{d}^T(\theta_k), \gamma^*(\theta_k)\mathbf{d}^H(\theta_k)]^T$. Then, the following optimization problem is obtained

$$\begin{aligned}\min_{\gamma(\theta_k)}\ I(\gamma(\theta_k)) = {}& \mathbf{d}^H(\theta_k)\mathbf{D}\mathbf{d}(\theta_k) + \gamma(\theta_k)\mathbf{d}^T(\theta_k)\mathbf{E}^*\mathbf{d}(\theta_k) +\\ & \gamma^*(\theta_k)\mathbf{d}^H(\theta_k)\mathbf{E}\mathbf{d}^*(\theta_k) + |\gamma(\theta_k)|^2\mathbf{d}^T(\theta_k)\mathbf{D}^*\mathbf{d}^*(\theta_k).\end{aligned} \tag{7}$$

Let the conjugate gradient of $I(\gamma(\theta_k))$ be equal to 0, thus, we get (6).

Subsequently, the C-IPNCM of $\mathbf{x}(t)$ can be reconstructed as

$$\tilde{\mathbf{Q}}_c = \sum\nolimits_{k=1}^{K} \frac{\gamma(\theta_k)\mathbf{d}(\theta_k)\mathbf{d}^T(\theta_k)}{\mathbf{d}^H(\theta_k)\hat{\mathbf{R}}_x^{-1}\mathbf{d}(\theta_k)} = \sum\nolimits_{k=1}^{K}\gamma(\theta_k)\varphi(\theta_k) \tag{8}$$

where $\varphi(\theta_k) = \frac{\mathbf{d}(\theta_k)\mathbf{d}^T(\theta_k)}{\mathbf{d}^H(\theta_k)\hat{\mathbf{R}}_x^{-1}\mathbf{d}(\theta_k)}$. In Xu's method [6], the spatial spectrum of noncircular coefficient $\tilde{\gamma}(\theta_k) = \gamma(\theta_k)\cdot\zeta(\theta_k)$, where $\zeta(\theta_k) = \frac{\mathbf{d}^H(\theta_k)\mathbf{d}(\theta_k)}{\mathbf{d}^H(\theta_k)(\mathbf{I}-\eta\hat{\mathbf{R}}_x^{-1})\mathbf{d}(\theta_k)}$, and η denotes the minimum eigenvalue of $\hat{\mathbf{R}}_{\tilde{x}}$. The difference between $\tilde{\gamma}(\theta_k)$ and $\gamma(\theta_k)$ is only the positive real coefficient $\zeta(\theta_k)$, i.e., $\mathsf{phase}[\tilde{\gamma}(\theta_k)] = \mathsf{phase}[\gamma(\theta_k)]$ and $|\tilde{\gamma}(\theta_k)| = \zeta(\theta_k)\cdot|\gamma(\theta_k)|$. There are three reasons why we choose $\gamma(\theta_k)$ to reconstruct the C-IPNCM. Firstly, the computational cost of $\gamma(\theta_k)$ is lower than $\tilde{\gamma}(\theta_k)$ since we don't need to calculate the minimum eigenvalue of $\hat{\mathbf{R}}_{\tilde{x}}$. Secondly, when $\theta_k \in \Theta_{in}$ $\big(\Theta_{in}$ denotes the angular set of the interference's directions$\big)$, $\eta\mathbf{d}^H(\theta_k)\hat{\mathbf{R}}_x^{-1}\mathbf{d}(\theta_k) \approx 0$ since the interference's power is always strong and η is a very small positive value, thus $\zeta(\theta_k) \approx 1 \Rightarrow |\gamma(\theta_k)| \approx |\tilde{\gamma}(\theta_k)|$, which means that (6) can accurately estimate the interference's noncircular rate. Thirdly, when $\theta_k \in \bar{\Theta} \setminus \Theta_{in}$, we have $\zeta(\theta_k) > 1$ due to $0 < \eta\mathbf{d}^H(\theta_k)\hat{\mathbf{R}}_x^{-1}\mathbf{d}(\theta_k) < N$, then $|\gamma(\theta_k)| < |\tilde{\gamma}(\theta_k)|$. Moreover, the reconstructed $\tilde{\mathbf{Q}}_c$ can be rewritten as $\tilde{\mathbf{Q}}_c = \tilde{\mathbf{Q}}_c^{\Theta_{in}} + \tilde{\mathbf{Q}}_c^{\bar{\Theta}\setminus\Theta_{in}}$, where $\tilde{\mathbf{Q}}_c^{\Theta_{in}} = \sum_{\theta_k\in\Theta_{in}}|\gamma(\theta_k)|^{j\cdot\mathsf{phase}[\gamma(\theta_k)]}\varphi(\theta_k)$, and $\tilde{\mathbf{Q}}_c^{\bar{\Theta}\setminus\Theta_{in}} = \sum_{\theta_k\in\bar{\Theta}\setminus\Theta_{in}}|\gamma(\theta_k)|^{j\cdot\mathsf{phase}[\gamma(\theta_k)]}\varphi(\theta_k)$. Therefore, compared with $|\tilde{\gamma}(\theta_k)|$, $|\gamma(\theta_k)|$ can reduce the proportion of $\tilde{\mathbf{Q}}_c^{\bar{\Theta}\setminus\Theta_{in}}$ in $\tilde{\mathbf{Q}}_c$, which results in $\tilde{\mathbf{Q}}_c$ closer to the theoretical C-IPNCM $\ddot{\mathbf{Q}}_c$, where $\ddot{\mathbf{Q}}_c = \sum_{p=2}^{P}\gamma_p\sigma_p^2\mathbf{a}_p\mathbf{a}_p^T + \sigma_n^2\mathbf{I}$, σ_p^2 is the power of the p-th interference, and σ_n^2 is the noise power.

The simulation results of Fig. 1 are added to verify the above analyses. Three signal sources come from the directions 3°, 30°, -40°, with the noncircularity rate 0.9, 1, 0.8, and the noncircularity phase -60°, 120°, 80°, respectively. The first signal source is the desired signal with SNR = 10 dB. The latter two are interferences and they have the same interference-to-noise ratios (INRs). It is easy to know that $\Theta_{in} = \{30^\circ, -40^\circ\}$. The angular sampling interval is 1°, and we set $\bar{\Theta} = [-90^\circ, -4^\circ] \cup [14^\circ, 90^\circ]$. Fig. 1 (a) compares the estimated spatial spectra of noncircularity rate between the proposed method (i.e. $|\gamma(\theta_k)|$) and the Xu's method (i.e. $|\tilde{\gamma}(\theta_k)|$). It can be observed that both the proposed method and the Xu's method can accu-

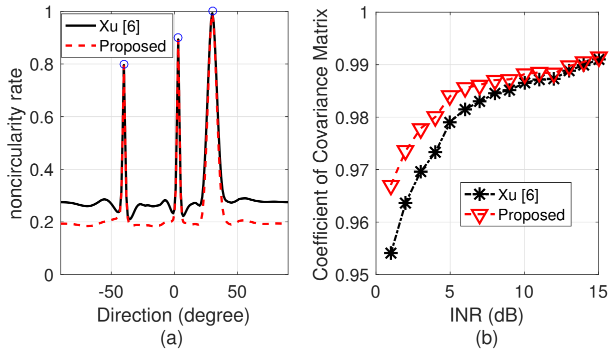

Fig. 1. (a): Spatial spectrum of noncircularity rate, SNR $=$ 10 dB, INR $=$ 10 dB; (b): Coefficient of covariance matrix versus input INR, SNR $=$ 10 dB.

rately estimate the noncircularity rate at the directions of interferences. When θ_k is close to the signal source's direction, $|\gamma(\theta_k)|$ and $|\tilde{\gamma}(\theta_k)|$ obtain almost the same value since $\mathbf{d}^H(\theta_k)\hat{\mathbf{R}}_x^{-1}\mathbf{d}(\theta_k) \approx 0 \Rightarrow \zeta(\theta_k) \approx 1$, while at other angles the values of $|\gamma(\theta_k)|$ are lower than $|\tilde{\gamma}(\theta_k)|$. In addition, the reconstruction performance of the C-IPNCM is evaluated by using the correlation coefficient between the reconstructed $\tilde{\mathbf{Q}}_c$ and the theoretical C-IPNCM $\ddot{\mathbf{Q}}_c$. The correlation coefficient is defined as $\mathrm{corr}(\tilde{\mathbf{Q}}_c, \ddot{\mathbf{Q}}_c) = \left|\mathrm{vec}(\tilde{\mathbf{Q}}_c)^H \mathrm{vec}(\ddot{\mathbf{Q}}_c)\right| / \left(\left\|\mathrm{vec}(\tilde{\mathbf{Q}}_c)\right\| \left\|\mathrm{vec}(\ddot{\mathbf{Q}}_c)\right\|\right)$ [16]. In Fig. 1 (b), we compare the correlation coefficient of the C-IPNCMs reconstructed by the proposed method and Xu's method to $\ddot{\mathbf{Q}}_c$ at different input INRs. It can be seen that when INR $\leq$ 12 dB, the correlation coefficients of the proposed method are larger than the Xu's method, which means that the C-IPNCM reconstructed by the proposed method is closer to the theoretical C-IPNCM.

Finally, the A-IPNCM of $\mathbf{x}(t)$ is reconstructed as

$$\tilde{\mathbf{R}}_{\mathbf{v}_\gamma} = \begin{bmatrix} \tilde{\mathbf{Q}}_r & \tilde{\mathbf{Q}}_c \\ \tilde{\mathbf{Q}}_c^* & \tilde{\mathbf{Q}}_r^* \end{bmatrix}. \tag{9}$$

3.2. The Desired Signal's ESV Estimation

Firstly, the subspace $\mathbf{U}$ is constructed to preprocess the received data, i.e., $\mathbf{U} = [\mathbf{u}_1, \mathbf{u}_2, \cdots, \mathbf{u}_{\tilde{P}}]$, where $\tilde{\mathbf{Q}}_r = \sum_{k=1}^{N} \lambda_k \mathbf{u}_k \mathbf{u}_k^H$, $\lambda_1 \geq \lambda_2 \geq \cdots \geq \lambda_N$ are the eigenvalues of $\tilde{\mathbf{Q}}_r$, $\mathbf{u}_k$ is the eigenvector associated with λ_k, and $\tilde{P}$ denotes the estimated number of the signal sources which can be calculated by the method of minimum description length (MDL) [17]. Generally speaking, the estimated value of $\tilde{P}$ has two situations since the interference signal sources are always strong, i.e., $\tilde{P} = P - 1$ (at low SNR) or $\tilde{P} = P$ (at high SNR). On the one hand, when $\tilde{P} = P - 1$, $\mathbf{U}$ is equivalent to the interference subspace. On the other hand, when $\tilde{P} = P$, $\mathbf{u}_1, \cdots, \mathbf{u}_{\tilde{P}-1}$ constitute the interference subspace, and $\mathbf{u}_{\tilde{P}}$ corresponds to a noise vector with $|\mathbf{u}_{\tilde{P}}^H \mathbf{a}_1|^2 \approx 0$. Moreover, according to [5], if interferences are not located at the main beam, we have $|\mathbf{a}_p^H \mathbf{a}_1|^2 \approx 0$ $(p = 2, 3, \cdots, P)$, which means that the desired signal's SV $\mathbf{a}_1$ is approximately orthogonal to the interference subspace. Therefore, based on the analyses above, whether the input SNR is high or not, $\mathbf{a}_1$ is approximately orthogonal to the subspace $\mathbf{U}$, i.e., $\mathbf{U}^H \mathbf{a}_1 \approx \mathbf{0}$. Thus, $(\mathbf{I} - \mathbf{U}\mathbf{U}^H)\mathbf{a}_1 = \mathbf{P}_{\mathbf{U}}^{\perp}\mathbf{a}_1 \approx \mathbf{a}_1$, where $\mathbf{P}_{\mathbf{U}}^{\perp} = \mathbf{I} - \mathbf{U}\mathbf{U}^H$ stands for the orthogonal projection matrix of $\mathbf{U}$. Secondly, project $\mathbf{x}(t)$ onto $\mathbf{P}_{\mathbf{U}}^{\perp}$, we can extract the SOI's component as

$$\check{\mathbf{x}}(t) = \mathbf{P}_{\mathbf{U}}^{\perp}\mathbf{x}(t) \approx \mathbf{a}_1 s_1(t) + \check{\mathbf{n}}(t), \tag{10}$$

where $\check{\mathbf{n}}(t) = \mathbf{P}_{\mathbf{U}}^{\perp}\mathbf{n}(t)$. The extended vector of $\check{\mathbf{x}}(t)$ is defined as

$$\tilde{\check{\mathbf{x}}}(t) = \left[\check{\mathbf{x}}^T(t), \check{\mathbf{x}}^H(t)\right]^T \approx \mathbf{a}_\gamma s_1(t) + \check{\mathbf{v}}_\gamma(t), \tag{11}$$

where $\check{\mathbf{v}}_\gamma(t) = \left[\check{\mathbf{n}}^T(t), \check{\mathbf{n}}^H(t) + \mathbf{h}^T(t)\right]^T$.

Next, we use the technique of shrinkage to estimate the desired signal's ESV. The cross correlation between $\tilde{\check{\mathbf{x}}}(t)$ and the WL beamformer's output $y(t)$ can be written as

$$\mathbf{f} = E\left[\tilde{\check{\mathbf{x}}}(t) y^*(t)\right], \tag{12}$$

where $y(t) = \mathbf{w}^H \tilde{\check{\mathbf{x}}}(t)$, $\mathbf{w}$ is the WL weighting vector. $s_1(t)$, $s_1'(t)$ and the noise are assumed to be independent from each other, and they all have zero mean. Substituting (11) into (12), $\mathbf{f}$ can be rewritten as

$$\mathbf{f} = E\left[\sigma_s^2 \mathbf{a}_\gamma^H \mathbf{w} \mathbf{a}_\gamma + \check{\mathbf{v}}(t)\check{\mathbf{v}}^H(t)\mathbf{w}\right]. \tag{13}$$

As we know, $|\mathbf{a}_\gamma^H \mathbf{w}| \gg |\check{\mathbf{v}}^H(t)\mathbf{w}|$, thus $\mathbf{f}$ is mainly determined by the first part. Then the more accurate estimate of $\mathbf{f}$ is, the better estimate of $\mathbf{a}_\gamma$ we will get.

Let us define $\hat{\mathbf{B}} = \hat{\kappa}\mathbf{I}$, where $\hat{\kappa} = \mathrm{Tr}(\hat{\mathbf{J}})/(2N)$, and $\hat{\mathbf{J}} = \mathrm{diag}(\tilde{\check{\mathbf{x}}} y^*)$. According to [18], a reasonable tradeoff between bias increase and covariance reduction can be obtained by the shrinkage of $\hat{\mathbf{J}}$ to $\hat{\mathbf{B}}$. Meanwhile, we can apply it in a vector shrinkage form

$$\hat{\mathbf{f}} = \hat{\rho}\,\mathrm{diag}(\hat{\mathbf{B}}) + (1 - \hat{\rho})\mathrm{diag}(\hat{\mathbf{J}}), \tag{14}$$

where $\hat{\rho}$ is the shrinkage coefficient.

Let $\hat{\mathbf{F}} = \mathrm{diag}(\hat{\mathbf{f}})$, then our goal is to compute the optimal value of $\hat{\rho}$ that minimizes the mean square error of $E\left[\left\|\hat{\mathbf{F}}(i) - \hat{\mathbf{B}}(i-1)\right\|_F^2\right]$ in the i-th snapshot. If we use the RBLW estimator, then (15) and (16) are obtained as

$$\hat{\mathbf{f}}_R(i) = \hat{\rho}_R(i)\mathrm{diag}\left[\hat{\mathbf{B}}(i)\right] + [1 - \hat{\rho}_R(i)]\mathrm{diag}\left[\hat{\mathbf{J}}(i)\right], \tag{15}$$

$$\hat{\rho}_R(i+1) = \min\left\{\frac{\frac{i-2}{i}\mathrm{Tr}\left[\hat{\mathbf{J}}(i)\hat{\mathbf{J}}^*(i)\right] + \varrho(i)}{(i+2)\mathrm{Tr}\left[\hat{\mathbf{J}}(i)\hat{\mathbf{J}}^*(i)\right] - \frac{\varrho(i)}{2N}}, 1\right\}, \tag{16}$$

or (17) and (18) can be obtained by using the OAS estimator

$$\hat{\mathbf{f}}_O(i) = \hat{\rho}_O(i)\mathrm{diag}\left[\hat{\mathbf{B}}(i)\right] + [1 - \hat{\rho}_O(i)]\mathrm{diag}\left[\hat{\mathbf{J}}(i)\right], \tag{17}$$

$$\hat{\rho}_O(i+1) = \frac{(1 - \frac{1}{N})\mathrm{Tr}\left[\hat{\mathbf{F}}(i)\hat{\mathbf{J}}^*(i)\right] + \varsigma(i)}{(i + 1 - \frac{1}{N})\mathrm{Tr}\left[\hat{\mathbf{F}}(i)\hat{\mathbf{J}}^*(i)\right] + (1 - \frac{i}{2N})\varsigma(i)}, \tag{18}$$

where $\hat{\mathbf{J}}(i) = \mathrm{diag}[\frac{1}{i}\sum_{t=1}^{i} \tilde{\check{\mathbf{x}}}(t) y^*(t)]$, $\varrho(i) = \mathrm{Tr}[\hat{\mathbf{J}}(i)]\mathrm{Tr}[\hat{\mathbf{J}}^*(i)]$,

Table 1. The steps of the the desired signal's ESV estimation.

1. Initialize: $\mathbf{w}(0) = \mathbf{1}$, $\hat{\rho}_R(1) = \hat{\rho}_O(1) = 0.8$

2. Repeat: For each snapshot index $i = 1, 2, \cdots$:

2-a: $y(t) = \mathbf{w}(i-1)^H \tilde{\mathbf{x}}(t)$

2-b: $\hat{\mathbf{J}}(i) = \mathrm{diag}\left[(1/i)\sum_{t=1}^{i} \tilde{\mathbf{x}}(t) y^*(t)\right]$

2-c: $\hat{\kappa}(i) = \mathrm{Tr}\left[\hat{\mathbf{J}}(i)\right]/(2N)$, $\hat{\mathbf{B}}(i) = \hat{\kappa}(i)\mathbf{I}$

2-d: calculate $\hat{\mathbf{f}}_R(i)$ and $\hat{\rho}_R(i+1)$ according to (15) and (16), respectively $\Big($or calculate $\hat{\mathbf{f}}_O(i)$ and $\hat{\rho}_O(i+1)$ according to (17) and (18), respectively$\Big)$

2-e: $\hat{\gamma}_s(i) = \hat{\mathbf{f}}_2^H(i)\hat{\mathbf{f}}_1^*(i)/[\hat{\mathbf{f}}_1^T(i)\hat{\mathbf{f}}_1^*(i)]$

2-f: $\tilde{\mathbf{a}}_\gamma(i) = \frac{\tilde{\hat{\mathbf{f}}}(i)}{\|\tilde{\hat{\mathbf{f}}}(i)\|}$, where $\tilde{\hat{\mathbf{f}}}(i) = [\hat{\mathbf{f}}_1^T(i), \hat{\gamma}_s^*(i)\hat{\mathbf{f}}_1^H(i)]^T$

2-g: $\mathbf{w}(i) = \tilde{\mathbf{R}}_{\mathbf{v}_\gamma}^{-1}\tilde{\mathbf{a}}_\gamma(i)/\left[\tilde{\mathbf{a}}_\gamma^H(i)\tilde{\mathbf{R}}_{\mathbf{v}_\gamma}^{-1}\tilde{\mathbf{a}}_\gamma(i)\right]$

and $\varsigma(i) = \mathrm{Tr}[\hat{\mathbf{F}}(i)]\mathrm{Tr}[\hat{\mathbf{F}}^*(i)]$. Moreover, if the initial value $\hat{\rho}_O(1)$ is between 0 and 1, the iterative process in (17) and (18) is guaranteed to converge [18]. It is easy to know that both $\mathbf{a}_\gamma$ and $\hat{\mathbf{f}}(i)$ can be divided into two parts

$$\mathbf{a}_\gamma = \left[\mathbf{a}_1^T, \mathbf{a}_2^T\right]^T \text{ and } \hat{\mathbf{f}}(i) = \left[\hat{\mathbf{f}}_1^T(i), \hat{\mathbf{f}}_2^T(i)\right]^T \tag{19}$$

where $\mathbf{a}_2 = \gamma_s^* \mathbf{a}_1^*$, and $\mathbf{a}_k \in C^{N\times 1}, \hat{\mathbf{f}}_k(i) \in C^{N\times 1} (k = 1, 2)$. Therefore, according to (13), if the estimated $\hat{\mathbf{f}}(i)$ is accurate enough, we have $\hat{\mathbf{f}}_2(i) = \gamma_s^* \hat{\mathbf{f}}_1^*(i)$. However, this situation will not happen due to the error of estimation, so the estimated $\hat{\mathbf{f}}(i)$ should be corrected. In order to correct the $\hat{\mathbf{f}}(i)$, we propose to minimize the following cost function

$$\min_{\gamma_s(i)} \left\|\hat{\mathbf{f}}_2(i) - \gamma_s^*(i)\hat{\mathbf{f}}_1^*(i)\right\|^2. \tag{20}$$

Then, $\hat{\gamma}_s(i) = \hat{\mathbf{f}}_2^H(i)\hat{\mathbf{f}}_1^*(i)/[\hat{\mathbf{f}}_1^T(i)\hat{\mathbf{f}}_1^*(i)]$. where $\hat{\gamma}_s(i)$ denotes the estimation of γ_s. Finally, the desired signal's SV is estimated as $\tilde{\mathbf{a}}_\gamma(i) = \tilde{\hat{\mathbf{f}}}(i)/\|\tilde{\hat{\mathbf{f}}}(i)\|$, where $\tilde{\hat{\mathbf{f}}}(i) = \left[\hat{\mathbf{f}}_1^T(i), \hat{\gamma}_s^*(i)\hat{\mathbf{f}}_1^H(i)\right]^T$. Throughout the above analysis, the steps of the ESV estimation are summarized in Table 1. Finally, the proposed weighting vector is calculated as

$$\mathbf{w}_{\mathrm{pro}} = \tilde{\mathbf{R}}_{\mathbf{v}_\gamma}^{-1}\tilde{\mathbf{a}}_\gamma/\left[\tilde{\mathbf{a}}_\gamma^H\tilde{\mathbf{R}}_{\mathbf{v}_\gamma}^{-1}\tilde{\mathbf{a}}_\gamma\right]. \tag{21}$$

where $\tilde{\mathbf{R}}_{\mathbf{v}_\gamma}^{-1} = \begin{bmatrix}\mathbf{D}_\mathbf{v} & \mathbf{E}_\mathbf{v} \\ \mathbf{E}_\mathbf{v}^* & \mathbf{D}_\mathbf{v}^*\end{bmatrix}$, $\mathbf{D}_\mathbf{v} = (\tilde{\mathbf{Q}}_r - \tilde{\mathbf{Q}}_c\tilde{\mathbf{Q}}_r^{*-1}\tilde{\mathbf{Q}}_c^*)^{-1}$, and $\mathbf{E}_\mathbf{v} = -\mathbf{D}_\mathbf{v}\tilde{\mathbf{Q}}_c\tilde{\mathbf{Q}}_r^{*-1}$.

Complexity analysis: the A-IPNCM reconstruction has a complexity of $O(KN^2)$. For the ESV estimation, the WL-OAS and the WL-RBLW share the same complexity of $O(LN^2)$. Therefore, the overall complexities of our proposed beamformers are equal to $O\left(\max\{KN^2, LN^2\}\right)$. The Xu's method [6] and the Huang's method [10] have the complexities of $O\left(\max\{KN^2, (2N)^{3.5}\}\right)$ and $O\left((L+2N)^{3.5}\right)$, respectively. The Zhang's method [12] and the NC-RCB [11] have the complexities of $O\left((2N)^{3.5}\right)$ and $O\left((2N)^3\right)$, respectively. Generally speaking, the computational cost of the proposed algorithms are lower than [6, 10, 12].

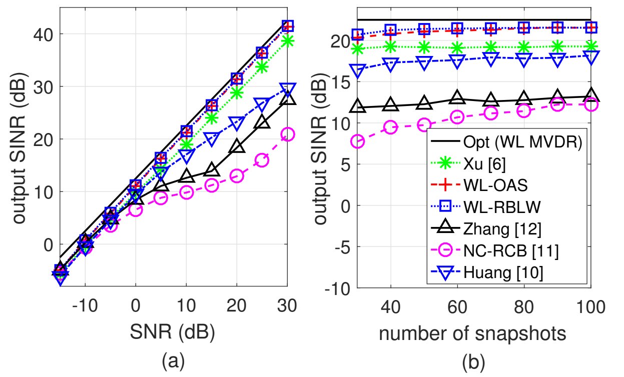

Fig. 2. (a): Output SINR versus input SNR; (b): Output SINR versus number of snapshots, SNR $= 10$ dB.

4. SIMULATION RESULTS

In the simulations, a uniform linear array (ULA) with 10 omni-directional sensors spaced half-wavelength distance is considered. The additive noise is modeled as complex circularly symmetric Gaussian zero-mean spatially and temporally white process. Three interferences come from the directions $30°, 64°, -45°$, with the noncircularity rate 1, 0.8, 0.9, and the noncircularity phase $-60°, 120°, 80°$, respectively. Their interference-to-noise ratios (INRs) are equal to 20 dB. The SOI is the UQPSK with $|\gamma_s| = 0.9$ and $\phi_s = 150°$, meanwhile, its presumed direction $\bar{\theta}_1 = 3°$. The angular region of the desired signal is set to be $\Theta = [-3°, 13°]$, and then $\bar{\Theta} = [-90°, -3°) \cup (13°, 90°]$. For the proposed methods, the parameters $\hat{\rho}_O(1) = \hat{\rho}_R(1) = 0.8$ and $\mathbf{w}(0) = \mathbf{1}$. The angular sampling interval in the whole spatial domain is 1°. The WL-RBLW and the WL-OAS are compared with the NC-RCB [11] with $\tilde{\epsilon} = 3$, the Xu's method [6], the Huang's method [10] with $\varepsilon_a = 0.25N = 2.5$ and $\varepsilon_\gamma = 0.1$, and the Zhang's method [12] with $\rho = 0.9$. The number of snapshots is 60. All the simulation figures are evaluated via 200 Monte Carlo independent runs, and the input SNR is fixed at 10 dB in Fig. 2 (b).

In Fig. 2, the random DOA mismatch of both the SOI and the interferences are uniformly distributed in $[-4°, 4°]$. It can be seen from Fig. 2 (a) that the WL-RBLW achieves the same performance as the WL-OAS, when SNR ≤ -5 dB, all the beamformers have similar performances, when SNR ≥ 0 dB, the output signal-to-interference-plus-noise ratios (SINRs) of the proposed beamformers are higher than the other competitors. From Fig. 2 (b), we can observe that the proposed algorithms outperform the other beamformers and can maintain their good performances even at a small number of snapshots.

5. CONCLUSIONS

In this paper, two new robust WL beamforming algorithms have been proposed for noncircular signals. Firstly, the A-IPNCM is reconstructed by using the spatial spectrum of noncircularity coefficient. Then, the RBLW estimator and the OAS estimator are modified to estimate the desired signal's ESV. Simulation results verify the effectiveness of the proposed beamformers.

6. REFERENCES

[1] B. Picinbono, "On circularity," *IEEE Trans. Signal Process.*, vol. 42, no. 12, pp. 3473–3482, 1994.

[2] P. Chevalier, J.P. Delmas, and A. Oukaci, "Properties, performance and practical interest of the widely linear MMSE beamformer for nonrectilinear signals," *Signal Process.*, vol. 97, no. 7, pp. 269–281, 2014.

[3] J. Liu, G. Gui, W. Xie, X. Cong, Q. Wan, and F. Adachi, "Robust widely linear beamforming via an iaa method for the augmented ipncm reconstruction," *IEICE TRANSACTIONS on Fundamentals of Electronics, Communications and Computer Sciences*, vol. 100, no. 7, pp. 1562–1566, 2017.

[4] P. Chevalier and A. Blin, "Widely linear MVDR beamformers for the reception of an unknown signal corrupted by noncircular interferences," *IEEE Trans. Signal Process.*, vol. 55, no. 11, pp. 5323–5336, 2007.

[5] D. Xu, L. Huang, X. Xu, and Z. Ye, "Widely linear MVDR beamformers for noncircular signals based on time-averaged second-order noncircularity coefficient estimation," *IEEE Trans. Veh. Technol.*, vol. 62, no. 7, pp. 3219–3227, 2013.

[6] D. Xu, C. Gong, S. Cao, X. Xu, and Z. Ye, "Robust widely linear beamforming based on spatial spectrum of noncircularity coefficient ," *Signal Process.*, vol. 104, no. 6, pp. 167–173, 2014.

[7] P. Chevalier, J. P. Delmas, and A. Oukaci, "Optimal widely linear MVDR beamforming for noncircular signals," in *Proc. of IEEE Int. Conf. Acoust., Speech, Signal Process. (ICASSP)*, 2009, pp. 3573–3576.

[8] P. Chevalier, J.P. Delmas, and A Oukaci, "Performance analysis of the optimal widely linear mvdr beamformer," in *Proc. of European Signal Processing Conference*, 2009, pp. 587–591.

[9] G.H. Wang, J.P. Lie, and C.M.S. See, "A robust approach to optimum widely linear MVDR beamformer," in *Proc. of IEEE Int. Conf. Acoust., Speech, Signal Process. (ICASSP)*, 2012, pp. 2593–2596.

[10] L. Huang, J. Zhang, L. Zhang, and Z.F. Ye, "Widely linear minimum dispersion beamforming for sub-Gaussian noncircular signals," *Signal Process.*, vol. 122, pp. 123–128, 2015.

[11] F. Wen, Q. Wan, H.W. Wei, R. Fan, and Y.J. Luo, "Robust Capon beamforming exploiting the second-order noncircularity of signals," *Signal Process.*, vol. 102, no. 102, pp. 100–111, 2014.

[12] J. Zhang, L. Huang, L. Zhang, and B. Zhang, "Robust widely linear beamformer based on a projection constraint," in *Proc. of IEEE Int. Conf. Acoust., Speech, Signal Process. (ICASSP)*, 2015, pp. 2509–2513.

[13] Y.J. Gu and A. Leshem, "Robust adaptive beamforming based on interference covariance matrix reconstruction and steering vector estimation," *IEEE Trans. Signal Process.*, vol. 60, no. 7, pp. 3881–3885, 2012.

[14] J. Liu, W. Xie, G. Gui, Q. Zhang, Y. Zou, and Q. Wan, "Adaptive beamforming algorithms with robustness against steering vector mismatch of signals," *IET Radar, Sonar & Navigation*, vol. 11, no. 12, pp. 1831–1838, 2017.

[15] Y.J Gu, N.A. Goodman, S.H. Hong, and Y. Li, "Robust adaptive beamforming based on interference covariance matrix sparse reconstruction," *Signal Process.*, vol. 96, no. 5, pp. 375–381, 2014.

[16] X.L. Yuan and L. Gan, "Robust adaptive beamforming via a novel subspace method for interference covariance matrix reconstruction," *Signal Process.*, vol. 130, pp. 233–242, 2017.

[17] M. Wax and T. Kailath, "Detection of signals by information theoretic criteria," *IEEE Trans. Acoust., Speech, Signal Process.*, vol. 33, no. 2, pp. 387–392, 1985.

[18] Y.L. Chen, A. Wiesel, and A.O. Hero, "Shrinkage estimation of high dimensional covariance matrices," in *Proc. of IEEE Int. Conf. Acoust., Speech, Signal Process. (ICASSP)*, 2009, pp. 2937–2940.